Supplementary Information

for

Bamboo-Inspired Anisotropic Hydrogels with Enhanced Mechanical Properties via Cellulose Nanocrystal-Reinforced Heterostructures

Pengyan Wu,[a] *Zhengjie Zhang,*[a] *Yan Hu,*[a] *Yan Li,*[a] *Tong Zhu,*[a] *Yanxi Liu,**[b] *Haitao Cui**[a] *and Haijun Cui**[a]

[a] Key Laboratory of Biorheological Science and Technology, Ministry of Education, College of Bioengineering, Chongqing University, Chongqing 400044, China.

[b] Institute of Pathology and Southwest Cancer Center, Southwest Hospital, Third Military Medical University (Army Medical University) and Key Laboratory of Tumor Immunopathology, Ministry of Education of China, Chongqing 400038, China.

*Corresponding author

E-mail: yanxi.liu341157@outlook.com; htcui.cbe@cqu.edu.cn;
haijuncui@cqu.edu.cn

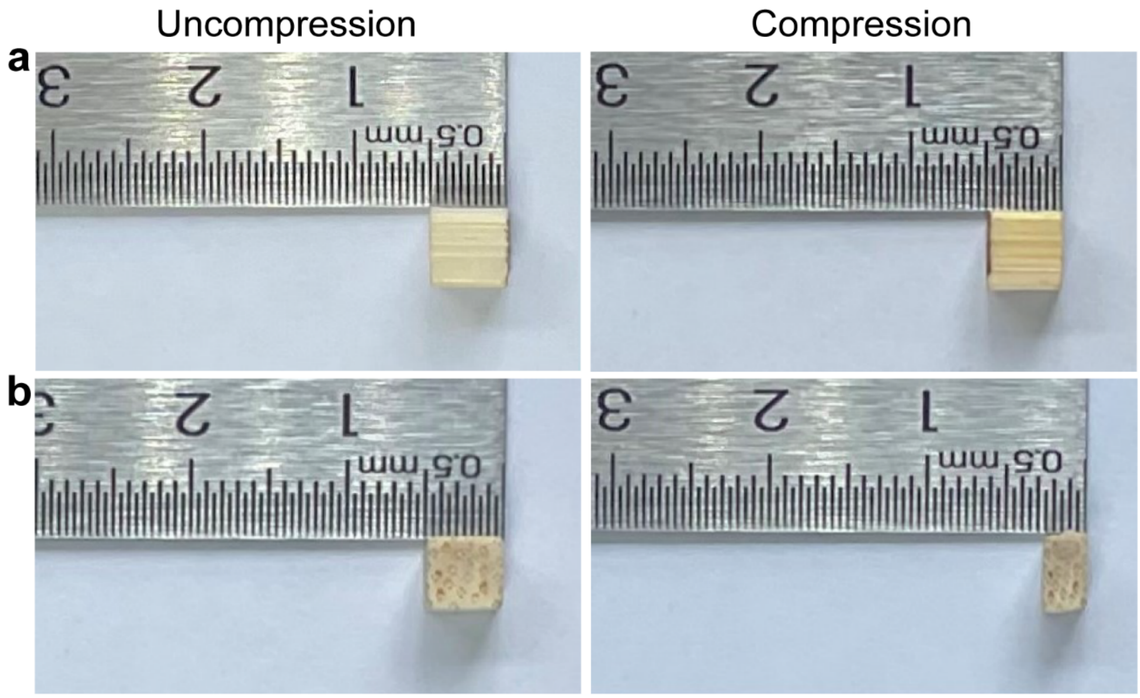

Fig. S1 Optical images of bamboo cubes before and after compression, with an initial dimension of 5 mm for each sample (a) Samples before and after axial compression. The size of the samples did not undergo obvious changes after axial compression. (b) Samples before and after radial compression. The sample underwent radial compression, resulting in a reduction in size.

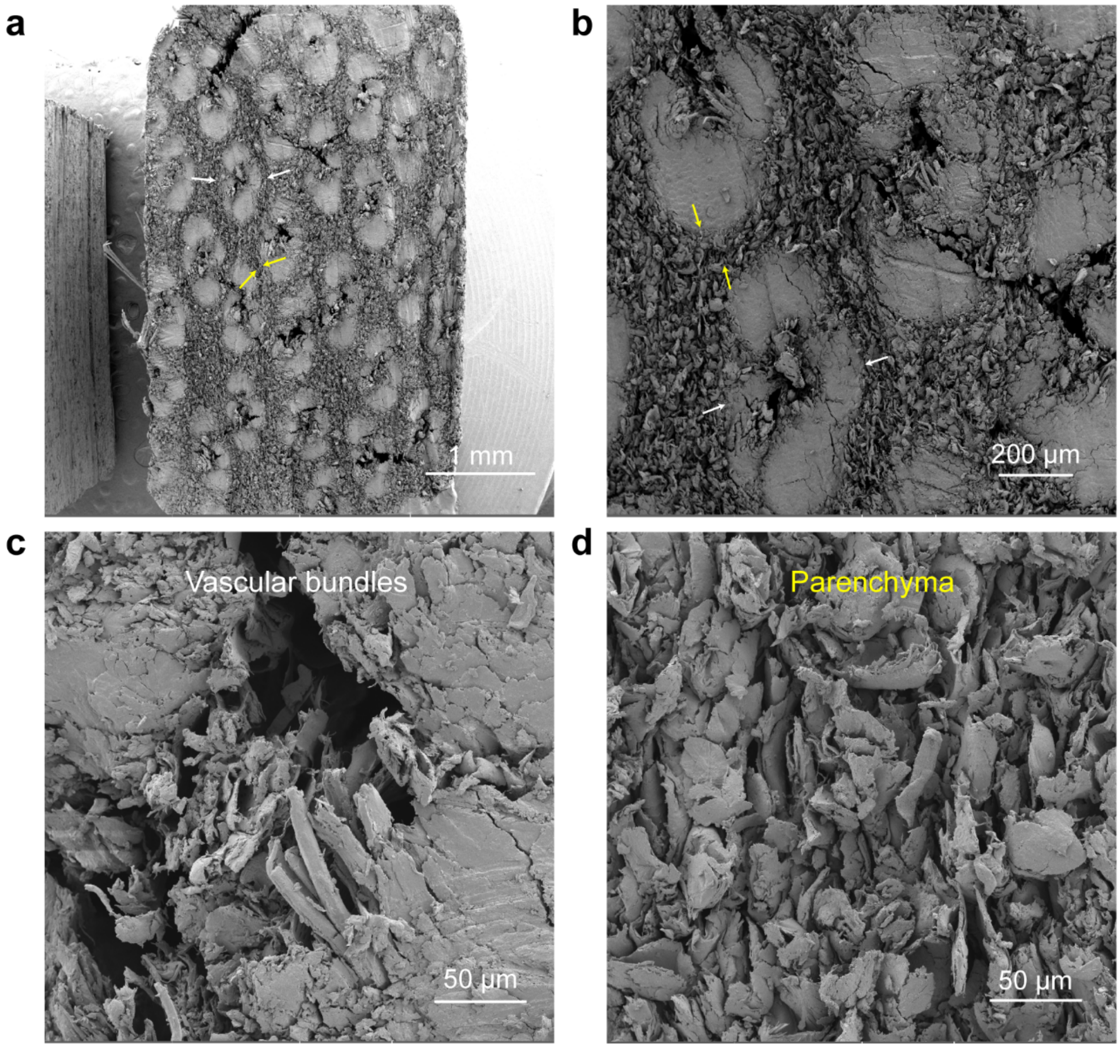

Fig. S2 Scanning Electron Microscopy (SEM) image of a radially compressed bamboo sample. The top panel presents an overview of the overall deformation of the bamboo structure following compression, illustrating macroscopic changes in fiber arrangement and surface morphology. The bottom panel offers a localized, enlarged view of the deformations occurring within the vascular bundles and parenchyma tissues, emphasizing the distinct structural responses of these components to the applied stress. Key features include the deformation of the vascular bundles, characterized by alterations in shape and orientation, as well as the compressive effects observed in the surrounding parenchyma tissues.

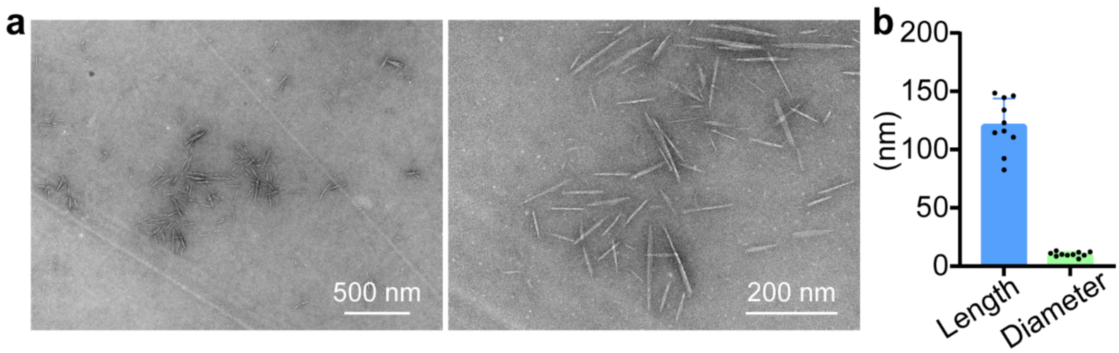

Fig. S3 Transmission Electron Microscopy (TEM) images of CNCs. (a) The morphology of CNCs under different magnifications. (b) The average length and average diameter of CNCs (n=10).

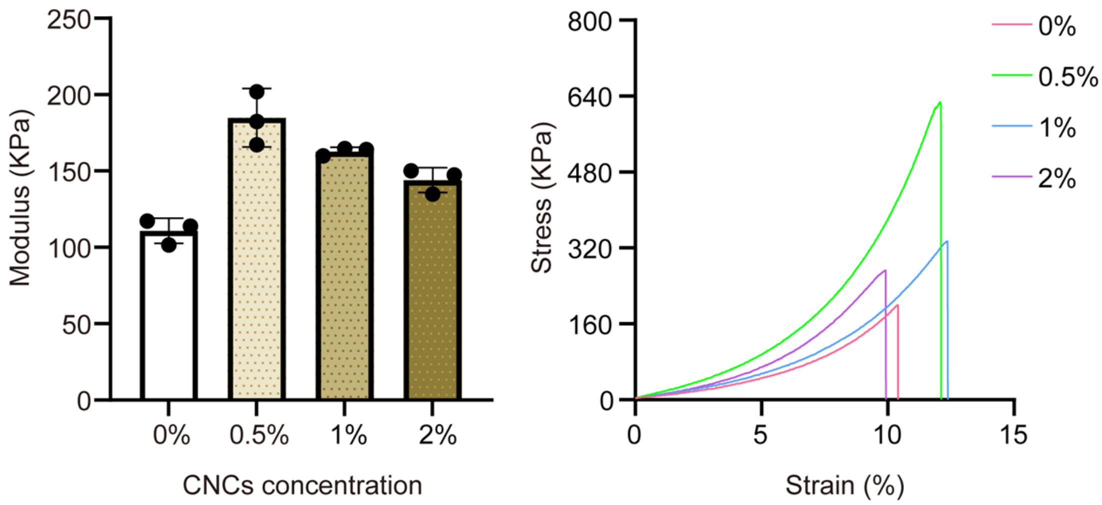

Fig. S4 Modulus changes and stress-strain curves of PEGDA hydrogels with different ratios of CNCs doping.

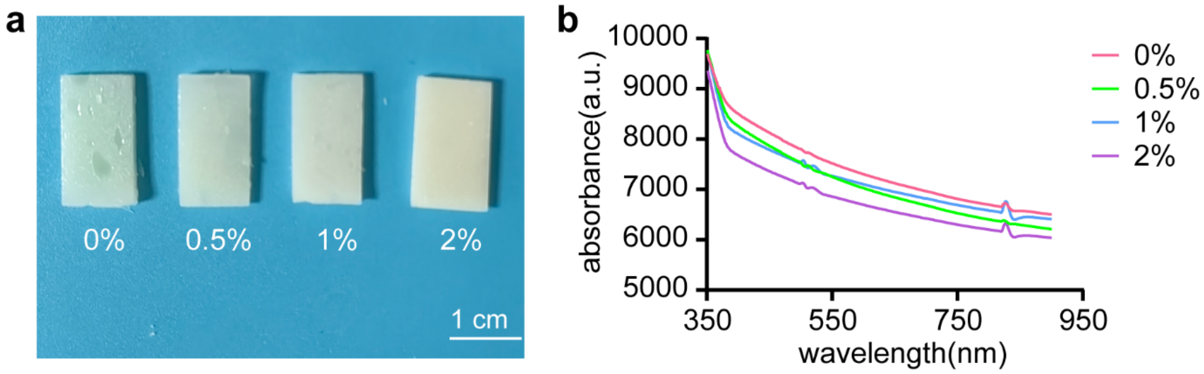

Fig. S5 UV absorption intensity of CNCs-doped hydrogels at different concentrations. (a) The hydrogel color darkens as the CNCs content increases, with the 2% CNCs-doped hydrogel appearing slightly yellowish. (b) The UV absorption intensity of the CNCs-doped pre-gel solution decreases with the increasing content. The pre-gel solution with 2% CNCs-doped exhibits weaker UV absorption than the 0% solution, likely due to lower polymerization efficiency, which could hinder more extensive polymerization of the hydrogel.

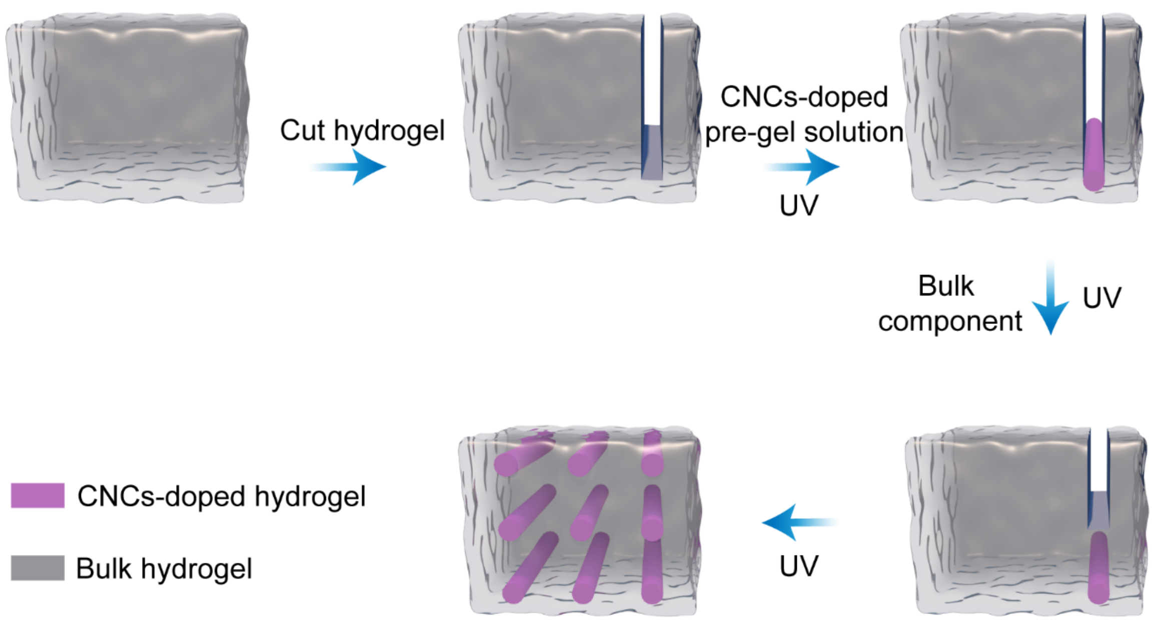

Fig. S6 Schematic illustration of the synthesis of biomimetic hydrogels. First, the square hydrogel is incised to form grooves. Subsequently, the CNCs-doped pre-gel solution is incorporated and subjected to UV for 3 minutes. Thereafter, the bulk component (CNCs-free) pre-gel solution is added. The above-mentioned steps are reiterated to synthesize biomimetic hydrogels with diverse fiber quantities.

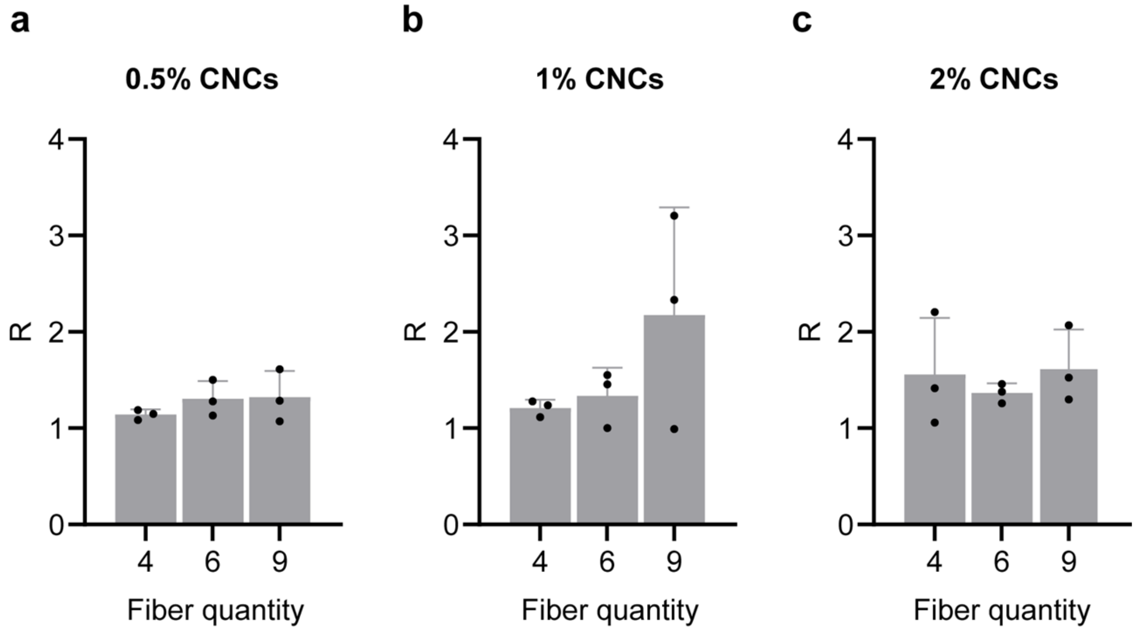

Fig. S7 The ratio of the axial modulus to the radial modulus of the biomimetic anisotropic hydrogel is defined as R. The results indicate that the R-value increases with the number of fibers, confirming the successful preparation of anisotropic hydrogels. The greater the number of CNCs fibers, the stronger the anisotropy.

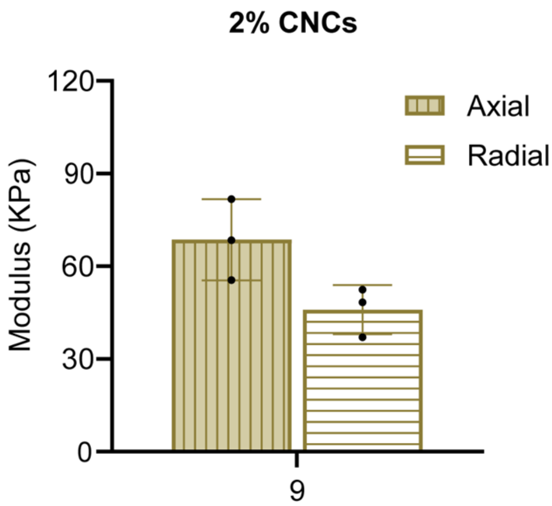

Fig. S8 The prepared PAA hydrogels exhibited anisotropic properties, with the axial modulus exceeding that of the radial modulus. The CNCs concentration is 2%, and the number of fibers is 9. All other preparation methods were consistent with those used for PEGDA hydrogels.

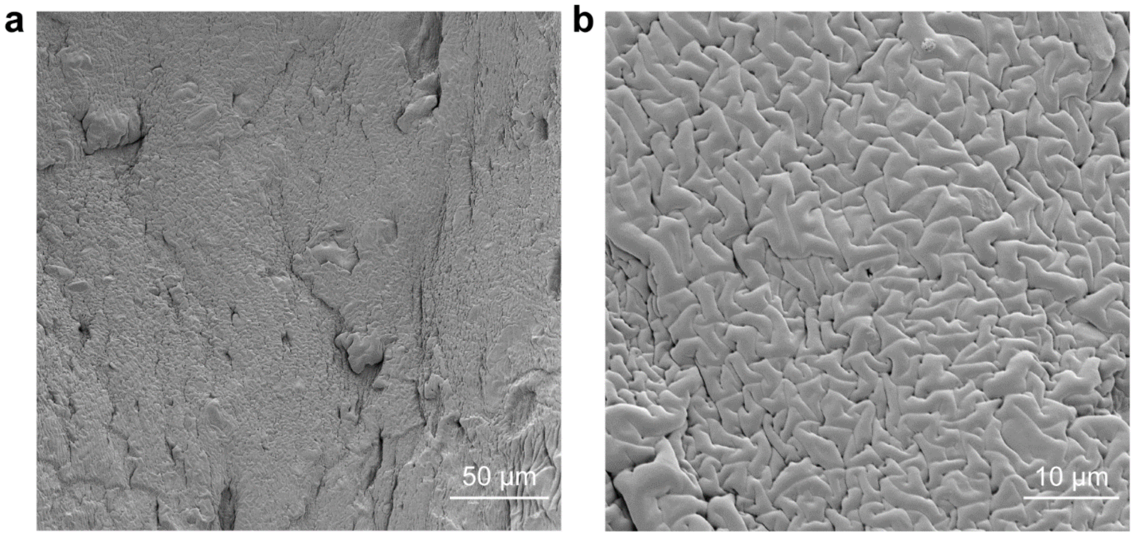

Fig. S9 SEM image of CNCs-doped PAA hydrogel after axial compression. The CNCs-doped PAA hydrogel generates a disordered stacking structure after axial compression, suggesting that the crystal alignment orientation of CNCs decreases after axial compression.

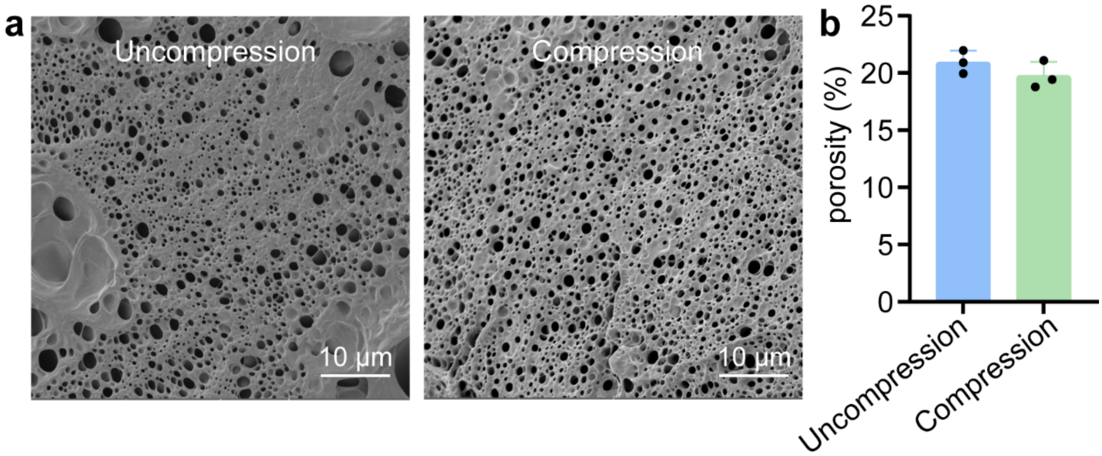

Fig. S10 The porosity of CNCs-free PAA hydrogel. (a) Owing to the excellent elastic behavior of the PAA hydrogel, the porosity of the CNCs-free PAA hydrogel did not undergo obvious changes after radial compression. (b) The porosity statistics of CNCs-free PAA hydrogels before and after compression (n=3).

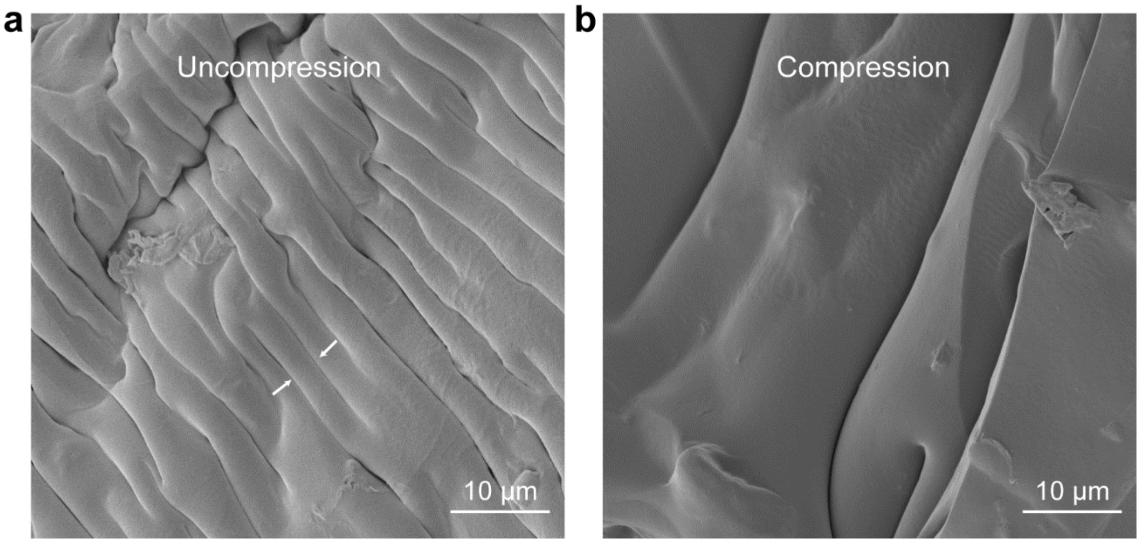

Fig. S11 SEM image of PAA hydrogel after radial compression. The cylindrical structure of the CNCs-doped hydrogel vanishes after compression, which might be attributed to the reorientation of CNCs upon exposure to radial pressure.

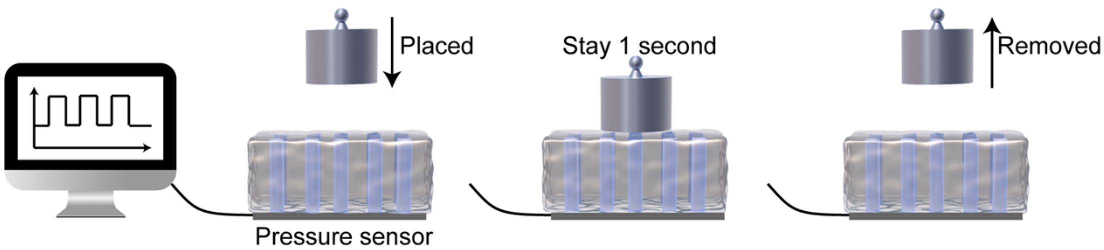

Fig. S12 Schematic illustration of mechanical sensing properties of anisotropic biomimetic hydrogels. The “Placed”, “Stay 1 second” and “Removed” process constitutes one single cycle, with each cycle last 2 seconds, for a total of 16 cycles.